Correlation between Unsteady-State Solidification Conditions, Dendrite Spacings, and Mechanical Properties of Al-Cu Alloys

JOSÉ M.V. QUARESMA, CARLOS A. SANTOS, and AMAURI GARCIA

The wide range of operational conditions existing in foundry and casting processes generates as a direct consequence a diversity of solidification microstructures. Structural parameters such as grain size and interdendritic spacings are strongly influenced by the thermal behavior of the metal/mold system during solidification, imposing, as a consequence, a close correlation between this system and the resulting microstructure. Mechanical properties depend on the microstructural arrangement defined during solidification. Expressions correlating the mechanical behavior with microstructure parameters should be useful for future planning of solidification conditions in terms of a determined level of mechanical strength, which is intended to be attained. In the present work, analytical expressions have been developed describing thermal gradients and tip growth rate during one-dimensional unsteady-state solidification of alloys. Experimental results concerning the solidification of Al-4.5 wt pct Cu and Al-15 wt pct Cu alloys and dendritic growth models have permitted the establishment of general expressions correlating microstructure dendrite spacings with solidification processing variables. The correlation of these expressions with experimental equations relating mechanical properties and dendrite spacings provides an insight into the preprogramming of solidification in terms of casting mechanical properties.

I. INTRODUCTION

AFTER casting, metallic alloys are generally used in one of four conditions: as-cast, heat treated after casting, mechanically worked after casting, and worked and heat treated. In all cases, the casting process has a significant influence upon the mechanical properties, especially in the former two cases. These properties are governed mainly by such factors as porosity, presence of a second phase, grain size, and dendrite spacings. While pouring molten metal from a ladle into a mold, a substantial amount of atmospheric air is entrained. The oxygen, nitrogen, and moisture in the entrained air react with molten metal and with mold coatings to form inclusions and porosity. These defects substantially lower the desired properties of cast metal, due primarily to stress concentration at the pores, which depends on pore shape, and to reduction in load-bearing area.[1–3]

It is generally found that the strength of a metallic material increases as the grain size decreases. The well-known Hall–Petch equation shows that the yield strength is proportional to the reciprocal of the square root of the grain diameter.[4,5] The improved properties of fine-grain-sized castings are due to the finer distribution of microporosity and second-phase particles. On the other hand, within each grain, there is a dendritic network, typified by a solute-poor region along the central dendrite axis. Moving away from this central area, the solute content will increase and microsegregation will occur between dendrite arms. In some cases, the interstices of the dendrites are sufficiently rich in solute that areas of nonequilibrium second phase or eutectic will form in a normally single-phase alloy. The outer boundary of this dendritic network will be the grain boundary, which will also be a preferred site for porosity, eutectic, or second-phase formations. For the as-cast, as well as the heat-treated or mechanically worked conditions, the fineness of the casting structure is recognized to yield superior mechanical properties to coarser ones, notably with respect to tensile strength and ductility. Figure 1 shows a schematic representation of a typical as-cast microstructure, with a grain boundary, a dendritic array, a second phase, and a porosity distribution.

The dendrite fineness can be of even more importance in the prediction of mechanical properties than in the prediction of grain size. Consequently, to control the properties of cast alloys, it is necessary to understand the mechanism and characterization of primary and secondary dendrite spacings during the solidification of alloys. Numerous studies have been carried out with a view to characterize such structure parameters. The studies can be grouped into two categories: solidification in steady-state heat flow and solidification in the unsteady-state regime.[6–12] Reliable spacing prediction in the latter category is of prime importance, since this class of heat flow regime encompasses the majority of industrial solidification processes.

The present article focuses on the relationships between solidification conditions, dendrite structure, and mechanical properties of cast Al-Cu alloys. Primary and secondary dendrite arm spacings have been linked to other solidification thermal parameters, such as dendritic tip velocity and temperature gradient in the solidifying material, as a function of distance from the chill surface. Based on mathematical models of heat transfer and dendritic growth during unsteady-state solidification, expressions have been developed correlating

JOSÉ M.V. QUARESMA, formerly Graduate Research Assisant, Department of Materials Engineering, State University of Campinas, UNICAMP, is Associate Professor, Department of Mechanical Engineering, Federal University of Para, Para, Brazil. CARLOS A. SANTOS, Research Assistant, and AMAURI GARCIA, Professor, are with the Department of Materials Engineering, State University of Campinas, UNICAMP, 13-083-970, Campinas-SP, Brazil.

Manuscript submitted May 1, 2000.

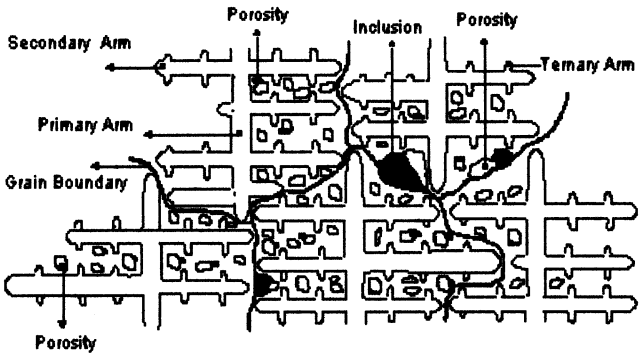

Fig. 1—Schematic representation of a typical as-cast microstructure.

the ultimate tensile strength and elongation as a function of variables of the metal/mold system.

II. EFFECTS OF SOLIDIFICATION CONDITIONS ON MICROSTRUCTURE

A. *Dendrite Spacings*

The primary and secondary arm spacings (λ_1 and λ_2) are important characteristics of dendritic microstructures and can have a marked effect on structure-mechanical properties relations. Many solidification studies have been reported in the literature, which characterize the variation of dendrite spacings with alloy composition, solidification rate (V), and temperature gradient (G) in the liquid, involving both solidification in state-steady heat flow[6–8] and that in the unsteady-state regime.[9] In the latter, which is the focus of this article, dendrite spacings are usually expressed as a function of cooling rate, GV, according to a power law given by

$$\lambda_{1,2} = C(GV)^{-a} \qquad [1]$$

where C is a constant and the exponent a has been recently summarized in the literature for a number of alloys.[9]

In a recent study, Hunt and Lu[10] derived analytical expressions, which fit results furnished by a numerical model, describing steady-state or non-steady-state array growth of an axisymmetric cell or dendrite. It was found that the primary dendrite spacings can be fitted by an expression of the form[10]

$$\lambda_1' = 0.07798\, V'^{(a-0.75)}\, (V' - G')^{0.75}\, G'^{-0.6028} \qquad [2]$$

where

$$a = -1.131 - 0.1555 \log_{10}(G') - 0.007589 [\log_{10}(G')]^2 \qquad [3]$$

$$\lambda_1' = \frac{\lambda \Delta T}{\Gamma k_0} \qquad [4]$$

$$G' = \frac{G_L \Gamma k_0}{\Delta T^2} \qquad [5]$$

$$V' = \frac{V \Gamma k_0}{D \Delta T} \qquad [6]$$

and ΔT is the equilibrium alloy freezing range, G_L is the liquid temperature gradient in the front of the interface, Γ is the Gibbs–Thompson coefficient, D is the solute diffusivity, k_0 is the partition coefficient, and V is the growth rate. Equation [2] has been confirmed by Feng *et al.*[11] for the steady-state solidification of an Al-4.95 wt pct Zn alloy.

Bouchard and Kirkaldy[9] have derived heuristically a spacing formula for steady-state solidification, which, modified by a dimensionless leading coefficient a_1, has proved its utility in the unsteady regime. The mentioned semiempirical formula is given by

$$\lambda_1 = a_1 \cdot \left(\frac{16 C_0^{1/2} (G_0 \varepsilon)\, \sigma_{SL} T_F D_L}{(1 - k_0)\, m_L \rho\, L G_L V_L} \right)^{1/2} \qquad [7]$$

where C_0 is the solute composition, σ_{SL} is the liquid-solid surface energy, $G_0\, \varepsilon$ is a characteristic parameter $\approx 600 \times 6$ K cm^{-1}, T_F is the fusion temperature of the solvent, D_L is the chemical diffusivity of the solute in the liquid, m_L is the liquidus slope, ρ is the density, L is the latent heat of fusion, and V_L is the tip growth rate.

For secondary dendrite spacings, Bouchard and Kirkaldy[9] derived an expression, which is very similar to the Mullins and Sekerka[12] temperature-gradient-independent marginal wavelength formula, which is given by

$$\lambda_2 = 2\pi a_2 \left(\frac{4 \sigma_{SL}}{C_0 (1 - k_0)^2 \rho L} \left(\frac{D_L}{V_L} \right)^2 \right)^{1/3} \qquad [8]$$

where a_2 is the secondary dendrite-calibrating factor.

B. *Determination of the Control Thermal Parameters G and V in One-Dimensional Unsteady-State Solidification*

An analytical heat transfer model, which describes the temperature distribution and the position of solidus and liquidus isotherms in the unidirectional solidification of binary alloys, will be used for determining expressions for G and V. The model is an extension of the one developed earlier by Garcia and Prates[13] for pure metals cooled by fluids and for pure metals solidifying against a massive uncooled mold.[14] The model employs the mathematically expedient technique of replacing the interfacial resistance by equivalent layers of material, and the latent heat of fusion is taken into account by adjusting the specific heat over the solidification temperature range. The ingot is treated as a one-dimensional moving boundary problem with boundaries at the tips and roots of the dendrites. It is assumed that the Newtonian interface resistance is represented by a metal/mold heat transfer coefficient h_i. The other thermophysical properties describing the system are treated as averages within the same phase, as follows:

$$T > T_{\text{Liq}} \qquad k_L,\ \rho_L,\ c_L \qquad [9]$$

$$T_{\text{Sol}} < T < T_{\text{Liq}} \qquad k_{SL} = (k_S + k_L)/2 \qquad [10]$$

Metal:

$$\rho_{SL} = (\rho_S + \rho_L)/2 \qquad [11]$$

$$c_{SL} = c_L + L/(T_{\text{Liq}} - T_{\text{Sol}}) \qquad [12]$$

$$T < T_{\text{Sol}} \qquad k_S,\ \rho_S,\ c_S \qquad [13]$$

where k is the thermal conductivity, c is the specific heat, T_{Liq} is the liquidus temperature, and T_{Sol} is the nonequilibrium solidus temperature.

The one-dimensional Fourier field equation is exactly applicable to the virtual metal/mold system, and the solution obtained in the system can be related to the real system by simple relationships. Under these assumptions, the model is completely described by the following equations.

Position of solidus isotherm:

$$t = \frac{S_S^2}{4\ \alpha_S\ (\phi_1)^2} + \frac{L_0 S_S}{2\ \alpha_S\ (\phi_1)^2} + \frac{(L_0^2 - S_0^2)}{4\ \alpha_S\ (\phi_1)^2} \qquad [14]$$

where t is time, S_S is the position of the solidus isotherm from the metal/mold interface, α_S is the solid diffusivity, ϕ_1 is a solidification constant associated with the displacement of solidus isotherm, S_0 is the thickness of the solid pre-existing adjunct to the metal in the virtual system, and L_0 is the thickness of the total pre-existing adjunct to metal in the virtual system (solid and mushy).

Position of liquidus isotherm:

$$t = \frac{S_L^2}{4\ \alpha_{SL}\ (\phi_2)^2} + \frac{L_0 S_L}{2\ \alpha_{SL}\ (\phi_2)^2} \qquad [15]$$

where S_L is the position of the liquidus isotherm from the metal/mold interface, α_{SL} is the mushy zone diffusivity, and ϕ_2 is a solidification constant associated with the displacement of the liquidus isotherm.

Temperature distribution in the mold (T_M):

$$T_M = T_0 + \frac{M(T_{\text{Sol}} - T_0)}{M + \text{erf}\ (\phi_1)} \left[1 + \text{erf}\left(N\phi_1 \frac{x - E_0}{S_S + L_0}\right)\right] \qquad [16]$$

where M is the ratio of heat diffusivities of the solid and mold material, $(k_S c_S \rho_S / k_M c_M \rho_M)^{1/2}$; N is the square root of the ratio of thermal diffusivities of the solid metal and mold material, $(\alpha_S/\alpha_M)^{1/2}$; E_0 is the thickness of the pre-existing adjunct to mold in the virtual system; T_0 is the environment temperature; and x is the position from the metal/mold interface.

Temperature distribution in the solid (T_S):

$$T_S = T_0 + \frac{(T_{\text{Sol}} - T_0)}{M + \text{erf}\ (\phi_1)} \left[M + \text{erf}\left(\phi_1 \frac{x + L_0}{S_S + L_0}\right)\right] \qquad [17]$$

Temperature distribution in the mushy zone (T_{SL}):

$$T_{SL} = T_{\text{Liq}} - \frac{(T_{\text{Liq}} - T_{\text{Sol}})}{\text{erf}\ (\phi_2) - \text{erf}\ (n\phi_1)} \left[\text{erf}\ (\phi_2) - \text{erf}\left(\phi_2 \frac{x + L_0}{S_L + L_0}\right)\right] \qquad [18]$$

where n is the square root of the ratio of thermal diffusivities of the solid metal and mushy zone, $(\alpha_S/\alpha_{SL})^{1/2}$.

Temperature distribution in the liquid (T_L):

$$T_L = T_p - \frac{(T_p - T_{\text{Liq}})}{1 - \text{erf}\ (m\phi_2)} \left[1 - \text{erf}\left(m\phi_2 \frac{x + L_0}{S_L + L_0}\right)\right] \qquad [19]$$

where m is the square root of the ratio of thermal diffusivities of the mushy zone and liquid, $(\alpha_{SL}/\alpha_L)^{1/2}$, and T_P is the pouring temperature.

Heat balances performed at the solid/mushy and mushy/liquid interfaces permit constants ϕ_1 and ϕ_2 to be determined by the simultaneous solution of the resulting equations:

$$\frac{T_{\text{Liq}} - T_{\text{Sol}}}{\text{erf}\ (\phi_2) - \text{erf}\ (n\phi_1)} = \frac{k_S \exp\left[(n^2 - 1)\phi_1^2\right]}{k_{SL}\ n \cdot [M + \text{erf}\ (\phi_1)]} (T_{\text{Sol}} - T_0) \qquad [20]$$

$$\frac{T_{\text{Liq}} - T_{\text{Sol}}}{\text{erf}\ (\phi_2) - \text{erf}\ (n\phi_1)} = \frac{k_L\ m \exp\left[(1 - m^2)\phi_2^2\right]}{k_{SL}\ [1 - \text{erf}\ (m\phi_2)]} (T_P - T_{\text{Liq}}) \qquad [21]$$

The virtual adjuncts S_0, L_0, and E_0 can be expressed as a function of the metal/mold heat transfer coefficient and are, respectively, given by

$$S_0 = \frac{2\ k_S \phi_1\ (T_{\text{Sol}} - T_0)}{\sqrt{\pi}\ (T_{\text{Liq}} - T_0) \exp\ (\phi_1^2)\ [M + \text{erf}\ (\phi_1)]\ h_i} \qquad [22]$$

$$L_0 = \frac{\phi_2}{n\phi_1} S_0 \qquad [23]$$

$$E_0 = \frac{S_0}{N} \qquad [24]$$

The growth rate or velocity at the tips of dendrites can be derived from Eq. [15] and is given by

$$V_L = \frac{2 \cdot \alpha_{SL}\ \phi_2^2}{S_L + L_0} \qquad [25]$$

By introducing L_0 defined by Eq. [23] into Eq. [25], the following is obtained:

$$V_L = \frac{2\ \alpha_{SL}\ \phi_2^2}{\left[\dfrac{2\ k_S\ \phi_2\ (T_{\text{Sol}} - T_0)}{n\ \sqrt{\pi}\ (T_{\text{Liq}} - T_0) \exp\ (\phi_1^2)\ [M + \text{erf}\ (\phi_1)] h_i}\right] + S_L} \qquad [26]$$

Temperature gradients immediately at the left of the dendrite tips and at the right of the tip interface can be derived from Eqs. [18] and [19] and are, respectively, given by

$$G_{SL} = \left(\frac{\partial T_{SL}}{\partial x}\right) = \frac{2\ \phi_2\ (T_{\text{Liq}} - T_{\text{Sol}})}{\sqrt{\pi}\ [\text{erf}\ (\phi_2) - \text{erf}\ (n\phi_1)] \exp\ (\phi_2)^2\ (S_L + L_0)} \qquad [27]$$

$$G_L = \left(\frac{\partial T_L}{\partial x}\right) = \frac{2\ m\ \phi_2\ (T_p - T_{\text{Liq}})}{\sqrt{\pi}\ [1 - \text{erf}\ (m\ \phi_2)] \exp\ (m\ \phi_2)^2\ (S_L + L_0)} \qquad [28]$$

The growth rate at the dendrite tips, as well as its temperature gradients given respectively by Eqs. [26] through [28], can be inserted into Eqs. [7] and [8] permitting primary and secondary dendrite spacings to be analytically calculated for given metal/mold solidification parameters such as pouring temperature and metal/mold heat transfer coefficient h_i.

III. EXPERIMENTAL PROCEDURE

The casting assembly used in solidification experiments is shown in Figure 2. The main design criterion was to

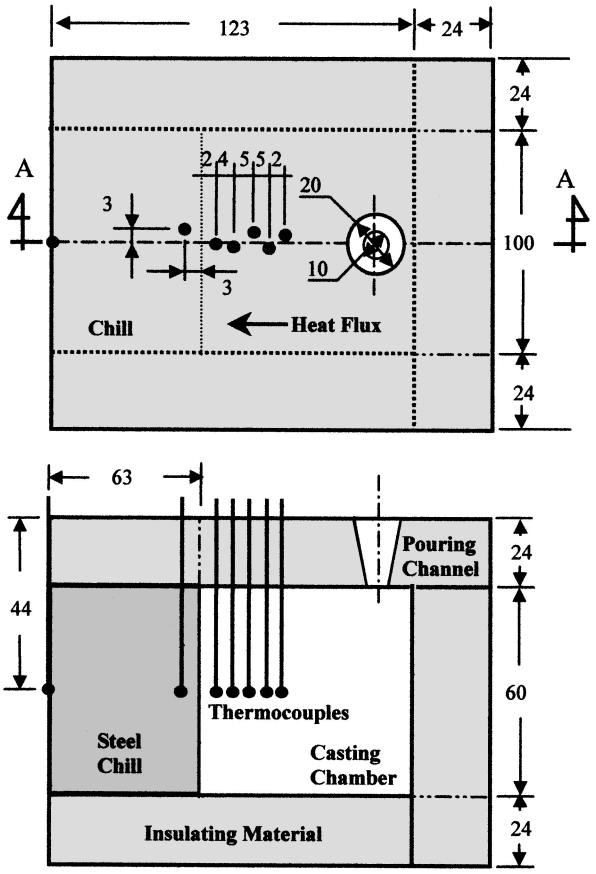

Fig. 2—Casting arrangement and position of thermocouples in mold wall and metal (mm).

ensure a dominant unidirectional heat flow during solidification. This objective was achieved by adequate insulation of the chill casting chamber. A low carbon steel chill was used, with the heat-extracting surface being polished. Experiments were performed with Al-4.5 wt pct Cu and Al-15 wt pct Cu alloys. The thermophysical properties of these alloys and chill are summarized in Table I.

Each alloy was melted in an electric resistance-type furnace until the molten metal reached a predetermined temperature. It was then stirred until the temperature was brought to a specific value, degassed with hexachloroethane tablets, and poured into the casting chamber with a superheat of 10 pct of the liquidus temperature. Temperatures in the chill and in the casting were monitored during solidification *via* the output of a bank of type *K* thermocouples (1.6-mm diameter) accurately located with respect to the metal/mold interface, as indicated in Figure 2. All the thermocouples were connected by coaxial cables to a data logger interfaced with a computer, and the temperature data were acquired automatically.

Longitudinal specimens were cut from the center of the solidified casting, as indicated in Figure 3. A selected section was electropolished and etched by an appropriate reagent (800 mL ethanol, 40 mL H_2O, and 60 mL perchloric acid) for metallographic examination. An image processing system Neophot 32 and Cambridge Leika-500 was then used to measure dendrite arm spacings (20 measurements) for each selected position from the metal/mold interface. Transversal specimens were cut from casting, as indicated in Figure 3, and prepared for tensile testing according to specifications of ASTM Standard E 8M.[21] To ensure reproducibility of results, four specimens were tested for each selected position, and mean values of ultimate tensile strengths and elongations have been determined at different positions with respect to the metal/chill interface.

IV. RESULTS AND DISCUSSION

The temperature files containing the experimentally monitored temperatures were used in a finite difference heat flow program to determine the transient metal/mold heat transfer coefficient, h_i, as described in previous articles.[19,20] Figure 4 shows typical examples of temperature data collected in metal and chill during the course of solidification of a Al-4.5 wt pct Cu alloy (Figure 4(a)) and a Al-15 wt pct Cu alloy (Figure 4(b)). These experimental thermal responses were compared to those numerically simulated by using the transient h_i profile, which provided the best curve fitting, yielding

$$\text{Al-4.5 wt pct Cu} \qquad h_i = 8650\ (t)^{-0.17}\ (\text{W/m}^2\ \text{K}) \qquad [29]$$

$$\text{Al-15 wt pct Cu} \qquad h_i = 17{,}000\ (t)^{-0.54} \qquad [30]$$

The results of thermal analysis in metal have also been used to determine the displacement of the liquidus isotherm, as well as the tip growth rate as a function of time and position, as indicated, respectively, in Figures 5 and 6. The Al-15 wt pct Cu alloy exhibits initial h_i values higher than those corresponding to the Al-4.5 wt pct Cu alloy, and as a direct consequence, the initial values of V_L are also higher for the former alloy. As solidification proceeds the interdendritic liquid feeds better the solidification contraction for alloys exhibiting a longer mushy zone, leading to higher values of h_i, and this translates to higher values of V_L for the Al-4.5 wt pct Cu alloy away from the chill.

The analytical expression for the growth rate derived in a previous section of this article (Eq. [26]) can be applied to the unidirectional solidification of both Al-Cu alloys examined and can be expressed as follows:

Al-4.5 wt pct Cu:

$$V_L = \frac{21\ \phi_2^2}{0.07415\ \dfrac{\phi_2}{\exp\ (\phi_1^2)\ [M + \text{erf}\ (\phi_1)]\ h_i} + S_L} \qquad [31]$$

Al-15 wt pct Cu:

$$V_L = \frac{13\ \phi_2^2}{0.06231\ \dfrac{\phi_2}{\exp\ (\phi_1^2)\ [M + \text{erf}\ (\phi_1)]\ h_i} + S_L} \qquad [32]$$

where V_L is in mm/s, S_L is in mm, and h_i is in W/mm^2 K.

Figure 7 illustrates values of constants ϕ_1 and ϕ_2 for Al-4.5 wt pct Cu and Al-15 wt pct Cu alloys for different molds and superheats.

Direct comparisons between experimental and calculated data using Eqs. [31] and [32] are illustrated in Figures 8(a) and (b). Relatively good agreements are observed in both cases, but the deviation increases for points approaching the casting surface, where theoretical values are higher than those observed experimentally.

Table I. Casting and Chill Materials Used for Experimentation and the Corresponding Thermophysical Properties[15–19]

Properties	Units	Al	Al-4.5 Wt Pct Cu	Al-15 Wt Pct Cu	Steel SAE 1010
Thermal conductivity	k_S (W/m · K)	222	193	179	46
	k_L	92	85	80	—
	k_{SL}	—	139	129	—
Specific heat	c_S (J/kg · K)	1123	1092	1080	527
	c_L	1086	1059	999	—
	c_{SL}	—	4996	6585	—
Density	ρ_S (kg/m^3)	2550	2680	2910	7860
	ρ_L	2380	2480	2760	—
	ρ_{SL}	—	2580	2835	—
Thermal diffusivity	α_S (m^2/s)	7.75×10^{-5}	6.63×10^{-5}	5.69×10^{-5}	—
	α_L	3.36×10^{-5}	3.24×10^{-5}	2.90×10^{-5}	—
	α_{SL}	—	1.07×10^{-5}	0.69×10^{-5}	—
Latent heat of fusion	L (J/kg)	385,000	381,900	374,270	—
Fusion temperature	T_F (°C)	660	660	660	—
Solidus temperature	T_{Sol} (°C)	—	548	548	—
Liquidus temperature	T_{Liq} (°C)	—	645	615	—
Solidification	ϕ_1	—	0.135	0.184	—
constant Eqs. [15] and [16]	ϕ_2	—	1.191	1.287	—
$(\alpha_S/\alpha_M)^{1/2}$	N	—	2.54	2.37	—
$(\alpha_S/\alpha_{SL})^{1/2}$	n	—	2.47	2.87	—
$(\alpha_{SL}/\alpha_L)^{1/2}$	m	—	0.577	0.480	—
$(k_S c_S \rho_S / k_M c_M \rho_M)^{1/2}$	M	—	1.64	1.64	—
Liquid-solid surface energy	σ_{SL} (J/m^2)	—	169×10^{-3}	169×10^{-3}	—
Solute diffusivity	D_L (m^2/s)	—	3.5×10^{-9}	3.5×10^{-9}	—
Solute composition	C_0 (wt pct)	—	0.045	0.15	—
Liquidus slope	m_L (°C/wt pct)	—	−2.6	−2.6	—
Partition coefficient	k_0	—	0.17	0.17	—

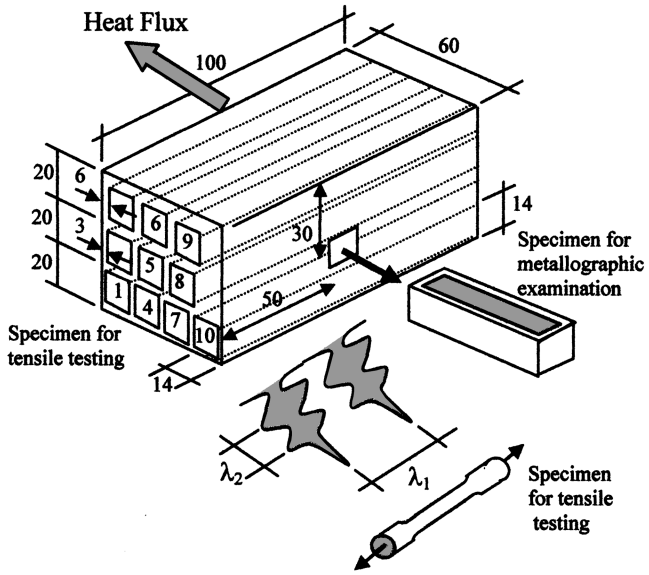

Fig. 3—Location of specimens for metallographic examination and tensile testing.

A significant part of such deviation may arise from the molten metal currents that are induced during progressive mold filling (not considered by the analytical approach, which assumes instantaneous mold filling) and that are more effective at the beginning of solidification. The latent heat evolution was handled in the analytical model by adjusting the specific heat over the solidification range, which can also contribute to deviations mainly for long freezing range alloys.

If both sides of Eqs. [27] and [28], which define the tip temperature gradients, are multiplied by a factor $\alpha_{SL}\phi_2$, these expressions become

$$G_{SL} = \left[\frac{(T_{\text{Liq}} - T_{\text{Sol}})}{\sqrt{\pi}\alpha_{SL}\ \phi_2\ [\text{erf}\ (\phi_2) - \text{erf}\ (n\phi_1)]\ \exp\ (\phi_2)^2}\right] \left[\frac{2\alpha_{SL}\phi_2^2}{(S_L + L_0)}\right] \quad [33]$$

$$G_L = \left[\frac{m\ (T_p - T_{\text{Liq}})}{\sqrt{\pi}\alpha_{SL}\ \phi_2\ [1 - \text{erf}\ (m\phi_2)]\ \exp\ (m\phi_2)^2}\right] \left[\frac{2\ \alpha_{SL}\phi_2^2}{(S_L + L_0)}\right] \quad [34]$$

It can be seen by comparing Eq. [25] with Eqs. [33] and [34] that both can be expressed as a function of tip growth rate. For a given metal/mold system, the first terms on the right-hand side of Eqs. [33] and [34] are constants represented below as C_1 and C_2 and the second term is the tip growth rate V_L, as given in Eq. [26]. For the present experimental investigations, these equations can be expressed as

Al 4.5 wt pct Cu:

$$G_L = 3.14\ (V_L) \quad [35]$$

$$G_{SL} = 1.64\ (V_L) \quad [36]$$

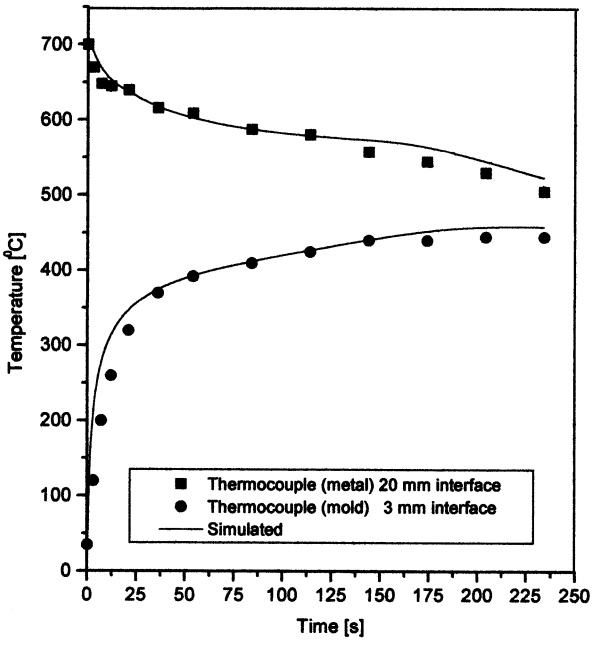

(*a*)

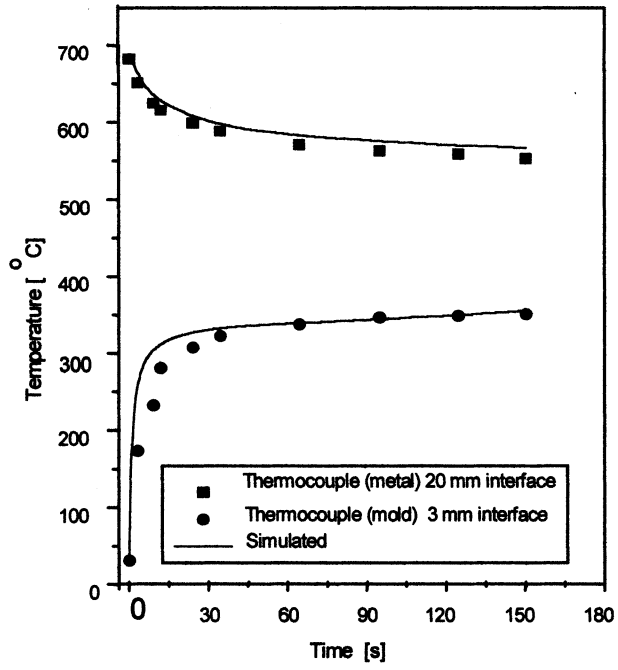

(*b*)

Fig. 4—Typical experimental thermal responses of thermacouples at two locations in casting and chill, compared to numerical simulations: (*a*) Al-4.5 wt pct Cu and (*b*) Al-15 wt pct Cu.

Al 15 wt pct Cu:

$$G_L = 3.25\ (V_L) \qquad [37]$$

$$G_{SL} = 2.09\ (V_L) \qquad [38]$$

where G_L and G_{SL} are in K/mm and V_L is in mm/s.

The last four equations define a linear variation between tip growth rate and temperature gradients, for solidification under unsteady-state heat flow conditions. Bouchard and

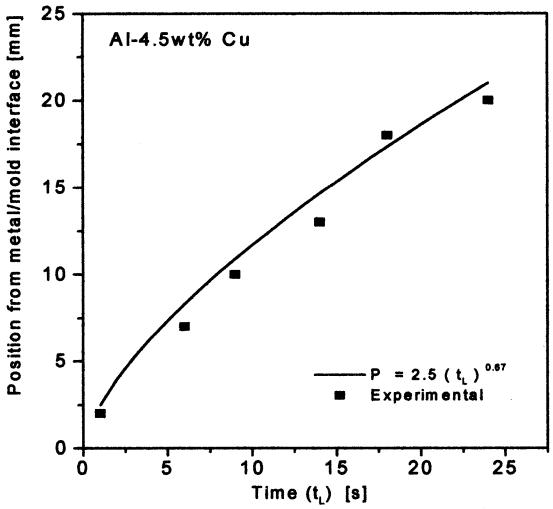

(*a*)

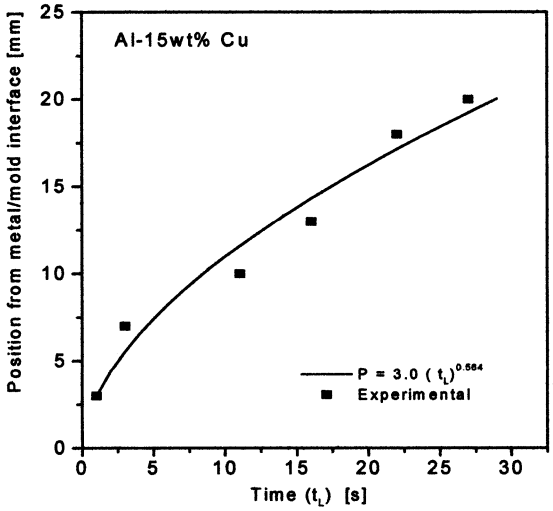

(*b*)

Fig. 5—Position of the liquidus isotherm as a function of time: (*a*) Al-4.5 wt pct Cu and (*b*) Al-15 wt pct Cu.

Kirkaldy in a recent article[9] have pointed out that the relationship between G_L or G_{SL} and V_L was observed to remain almost linear even when values of parameters such as metal/mold heat transfer coefficient, h_i, solute content and superheat were changed. Eqs. [35] through [38] demonstrate unambiguously that the relationship is actually linear, and Eqs. [33] and [34] show clearly where the aforementioned parameters are inserted. The metal/mold heat transfer coefficient is a variable appearing in Eq. [26], which defines V_L; the superheat affects the pouring temperature, T_P, as well as the constants ϕ_1 and ϕ_2; and the solute content will affect the solidification range and thermophysical properties.

As a consequence of this linear relationship, the cooling rate ($\mathring{T}$) of the dendrite tip will be given by an expression of the form

$$\mathring{T} = C_1\ V_L^2 \qquad [39]$$

Figures 9 and 10 show, respectively, experimental tip growth rate as a function of temperature gradients calculated according to expressions [35] through [38] and cooling rates

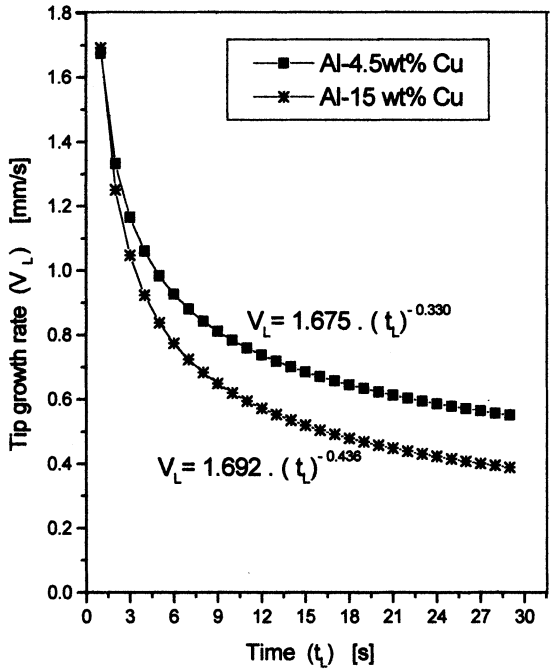

(*a*)

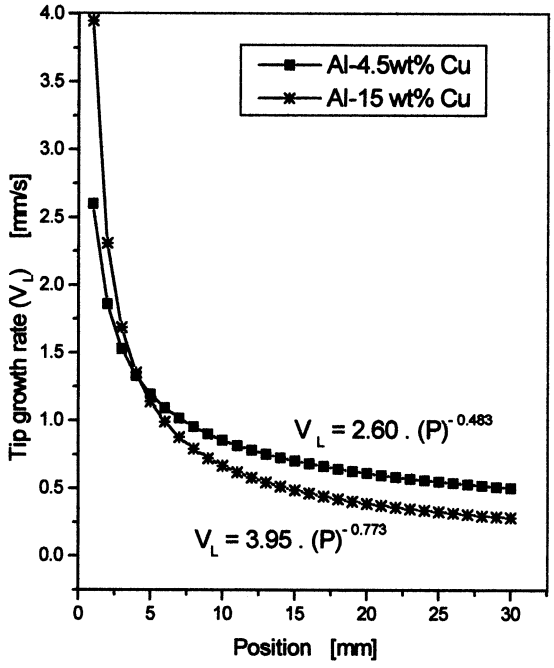

(*b*)

Fig. 6—Variation of the tip growth rate (V_L) with (*a*) time and (*b*) position from metal/mold interface in Al-4.5 wt pct Cu and Al-15 wt pct Cu.

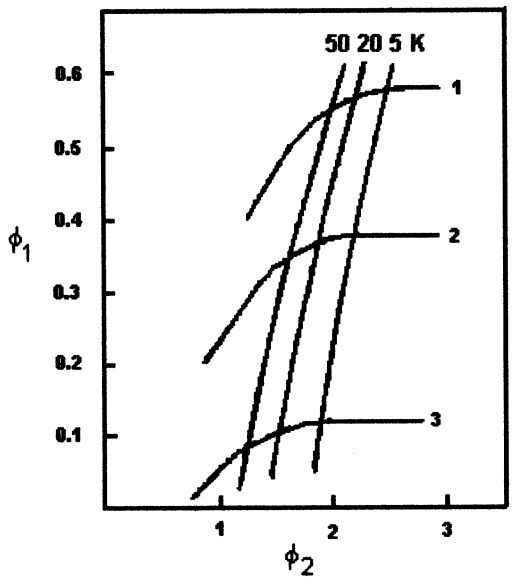

(*a*)

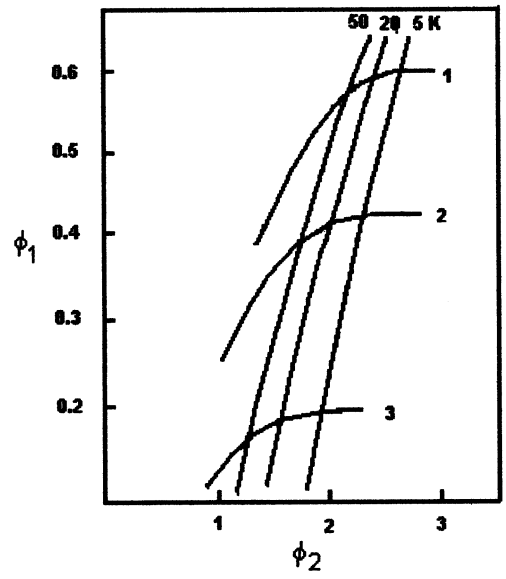

(*b*)

Fig. 7—Theoretical values of constants ϕ_1 and ϕ_1 for (*a*) Al-4.5 wt pct Cu and (*b*) Al-l5 wt pct Cu alloys: 1—steel mold, 2—copper mold, and 3—cooled mold. Superheats: 5, 20, and 50K.

as a function of experimental values of V_L and position from the metal/mold interface calculated by Eq. [39].

Figures 11 and 12 show, respectively, typical macrostructures and microstructures of Al-4.5 wt pct Cu and Al-15 wt pct Cu ingots. It can be seen that only Al-4.5 wt pct Cu presents a well-defined columnar zone followed by an equiaxed zone, while Al-15 wt pct Cu is completely equiaxed. As the primary dendrite spacings were only clearly defined in the columnar zone, micrographic data concerning this spacing were collected only in the former ingot. Secondary spacings were measured for both alloys.

Primary dendrite arm spacings (λ_1) were calculated by incorporating Eqs. [35] and [37], respectively, for Al-4.5 wt pct Cu and Al-15 wt pct Cu, as well as the corresponding experimental values of growth rate into Eq. [7] proposed by Bouchard and Kirkaldy.[9] Liquidus slope, alloy bulk compositions, and distribution coefficients were taken on a solute weight percent basis, as indicated in Table I, instead of a mole fraction basis, as originally used by Bouchard and Kirkaldy. The value of the dimensionless calibration parameter a_1 was found to be 50. The theoretical model of Hunt and Lu[10] represented by Eqs. [2] through [6] was also used to calculate λ_1 values as a function of tip growth rates. Predictions furnished by both theoretical models are plotted

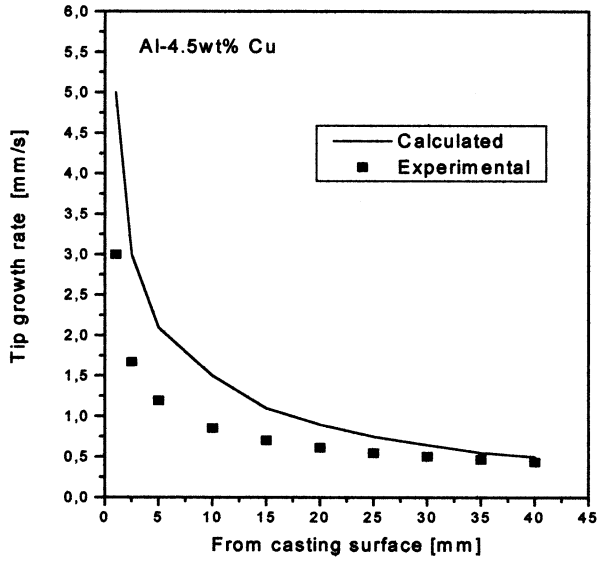

(*a*)

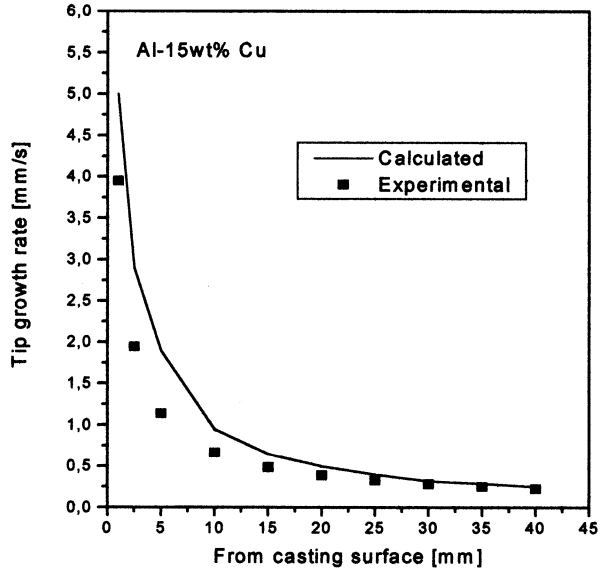

(*b*)

Fig. 8—Comparison between experimental and calculated growth rate: (*a*) Al-4.5 wt pct Cu and (*b*) Al-15 wt pct Cu.

against experimental spacings in Figure 13. A good agreement can be observed between experimental data and theoretical predictions of Bouchard and Kirkaldy's semiempirical approach with the suggested calibration coefficient. The model of Hunt and Lu predicts values of λ_1 far from those observed experimentally, but if the constant 0.07798 is multiplied by a factor of 6, an excellent agreement is attained, as shown in Figure 13. The slope of the theoretical equation representing this later model permits a better fit with the experimental results.

Figure 14 illustrates the calculated and measured secondary dendrite arm spacings at two different alloy compositions. The theoretical approach was that due to Bouchard and Kirkaldy[9] and represented by Eq. [8]. These authors suggest a calibrating factor a_2 ranging between 4 and 11 for a number of alloys, including the Al-Cu system. In our

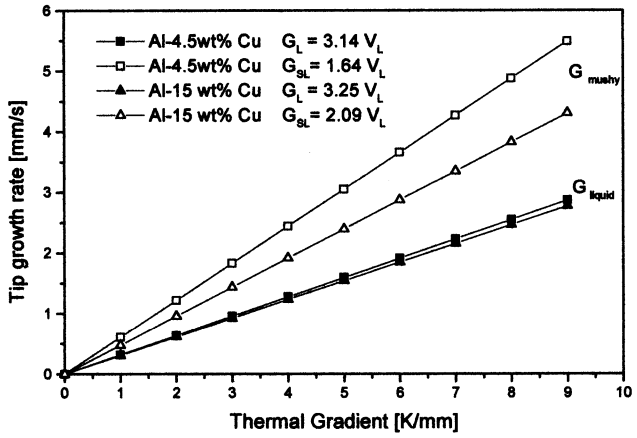

Fig. 9—Tip growth rate as a function of tip thermal gradient (superheat = 0.1 pct and T_{Liq}).

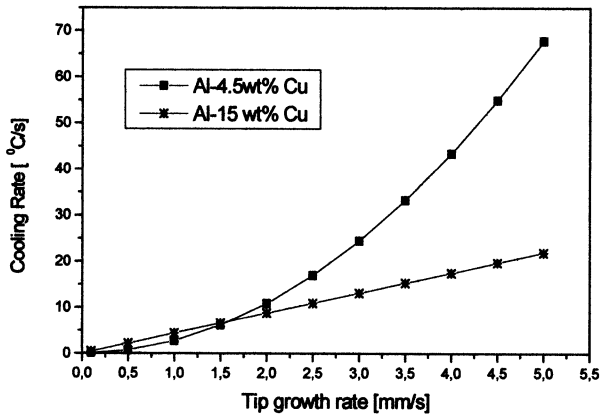

(*a*)

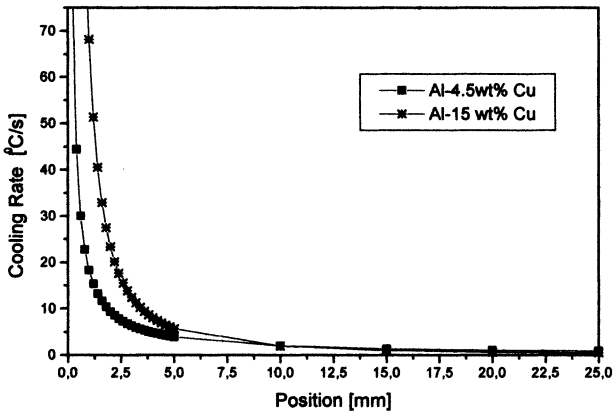

(*b*)

Fig. 10—Cooling rates as a function of experimental values of (*a*) V_L and (*b*) position from the metal/mold interface.

experimental investigation, a calibrating factor of 7.43 appears to be appropriated for both alloys examined, as indicated by the good agreement observed in Figure 14 between measured and calculated secondary spacings. These spacings were found to be related with tip growth rates according to

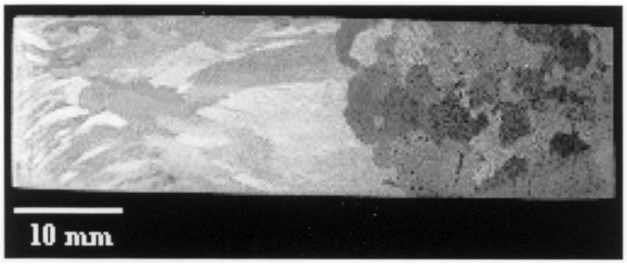

(*a*)

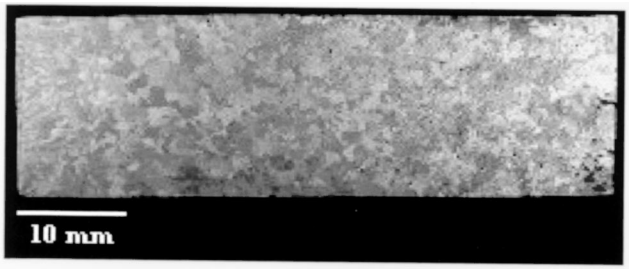

(*b*)

Fig. 11—Typical macrostructures of (*a*) Al-4.5 wt pct Cu and (*b*) Al-15 wt pct Cu ingots.

Al 4.5 wt pct Cu:

$$\lambda_2 = 29.9 \left(\frac{1}{V_L}\right)^{2/3} \quad [40]$$

Al-15 wt pct Cu:

$$\lambda_2 = 21.9 \left(\frac{1}{V_L}\right)^{2/3} \quad [41]$$

where λ_2 is in μm and V_L is in mm/s.

Although the preceding equations do not explicitly predict that the functional relationship of λ_2 with the cooling rate ($\mathring{T}$) is $-1/3$, it is implicit from the linear relationship between V_L and G_L (or G_{SL}), as defined by Eqs. [35] and [37].

As analytic expressions allow experimental results to be rapidly compared with theory, it seems convenient to obtain a general theoretical expression for λ_2. This can be done by incorporating Eq. [26] into Eqs. [40] and [41], yielding

Al-4.5 wt pct Cu:

$$\lambda_2 = 29.9 \left(\frac{S_L + 0.07415 \dfrac{\phi_2}{\exp(\phi_1^2)\,[M + \operatorname{erf}(\phi_1)]\,h_i}}{21\,\phi_2^2} \right)^{2/3} \quad [42]$$

Al-15 wt pct Cu:

$$\lambda_2 = 21.9 \left(\frac{S_L + 0.06231 \dfrac{\phi_2}{\exp(\phi_1^2)\,[M + \operatorname{erf}(\phi_1)]\,h_i}}{13\,\phi_2^2} \right)^{2/3} \quad [43]$$

where λ_2 is in μm and h_i is in W/mm^2 K.

These equations permit λ_2 to be determined as a function of metal/mold solidification parameters, represented by M, ϕ_1, ϕ_2, and h_i.

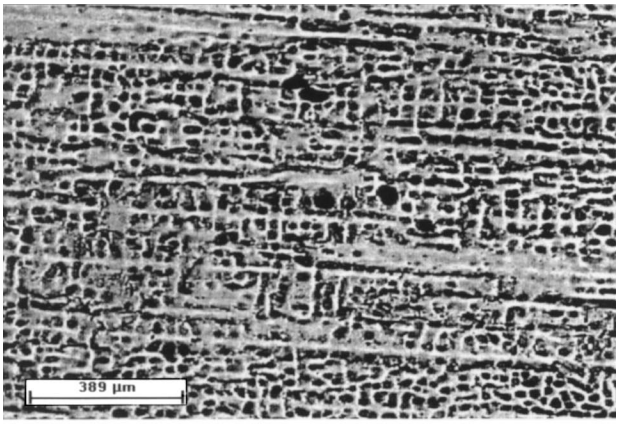

Al-4.5wt% Cu

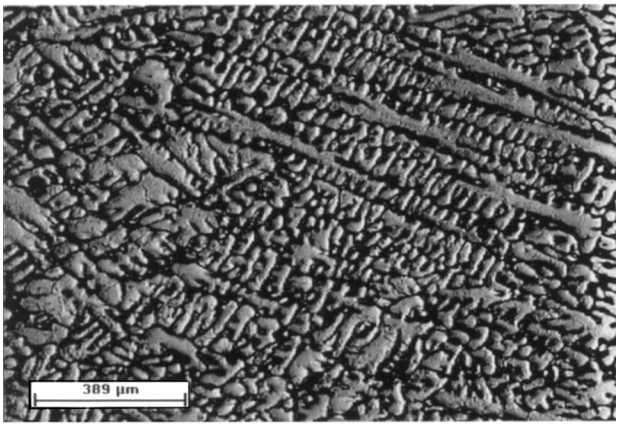

Al-15wt% Cu

Fig. 12—Typical microstructures of Al-4.5 wt pct Cu and Al-15 wt pct Cu ingots: 13 mm from metal/mold interface.

The results of the tensile data obtained in the various experiments are summarized in Figures 15 through 17. The mechanical properties, ultimate tensile strength, and elongation are related to the microstructural fineness, *i.e.*, primary and secondary dendrite spacings. These results appear consistent with the knowledge found in the literature relating microstructure effects with mechanical properties.

The results concerning elongation as a function of secondary dendrite spacings are limited to the Al-4.5 wt pct Cu alloy, due to the inherent brittle fracture of the Al-15 wt pct Cu specimens (Figure 18).

Analysis of the present results has suggested experimental equations relating the dependence of ultimate tensile strength and ductility on dendrite spacings. These equations shown in Figures 15 through 18 can incorporate Eqs. [42] and [43], yielding

Al-4.5 wt pct Cu:

$$\sigma_u = 46 + 145 \left(\frac{21\,\phi_2^2}{S_L + 0.07415 \dfrac{\phi_2}{\exp(\phi_1^2)\,[M + \operatorname{erf}(\phi_1)]\,h_i}} \right)^{1/3} \quad [44]$$

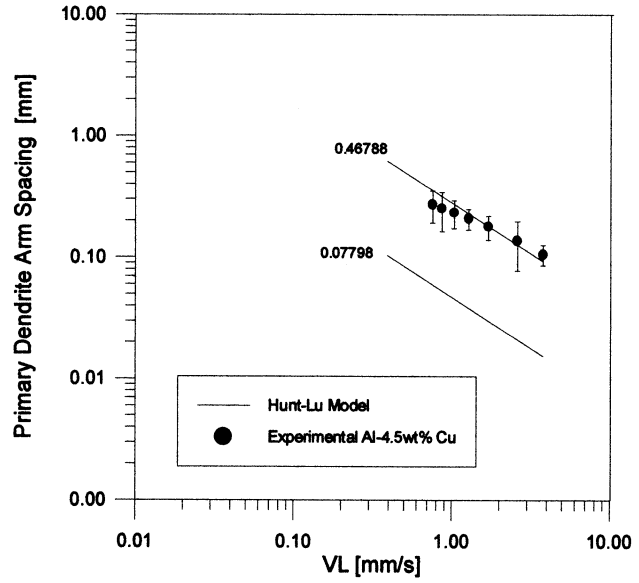

(*a*)

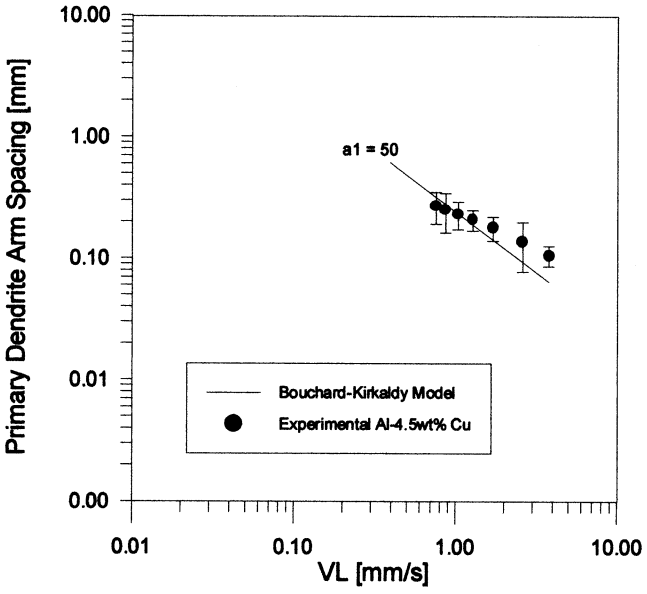

(*b*)

Fig. 13—Comparison between experimental and calculated λ_1 for A-4.5 wt pct Cu: (*a*) Hunt–Lu model[10] and (*b*) Bouchard–Kirkaldy model.[9]

$$\delta = 0.034 + 0.179 \left(\frac{21\ \phi_2^2}{S_L + 0.07415 \dfrac{\phi_2}{\exp(\phi_1^2)\,[M + \operatorname{erf}(\phi_1)]\,h_i}} \right)^{1/3} \quad [45]$$

Al-15 wt pct Cu:

$$\sigma_u = 78 + 148 \left(\frac{13\ \phi_2^2}{S_L + 0.06231 \dfrac{\phi_2}{\exp(\phi_1^2)\,[M + \operatorname{erf}(\phi_1)]\,h_1}} \right)^{1/3} \quad [46]$$

where σ_u is in MPa, S_L is in mm, h_i is in W/mm^2 K, and δ is in percent.

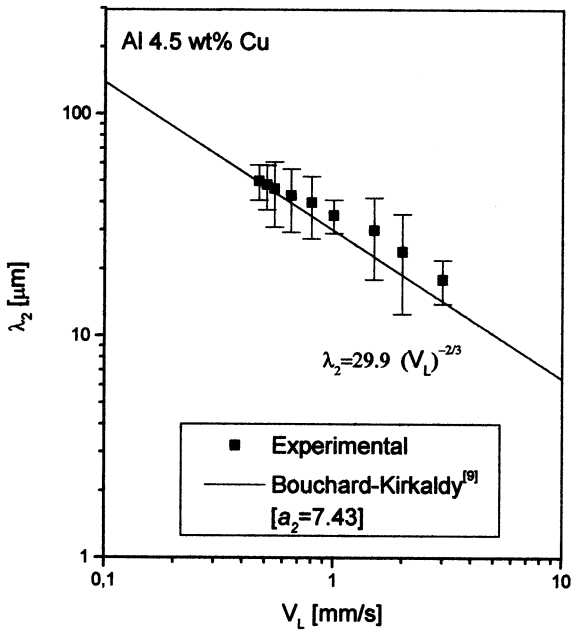

(*a*)

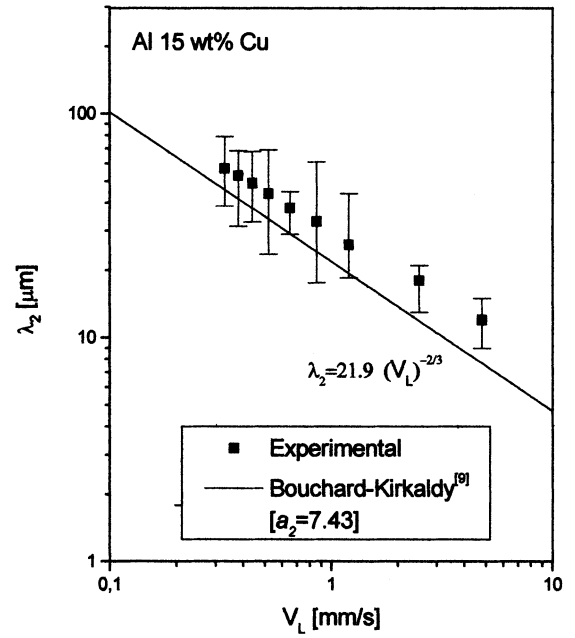

(*b*)

Fig. 14—Comparison between experimental and calculated secondary arm spacings: (*a*) Al-4.5 wt pct Cu and (*b*) Al-15 wt pct Cu.

These equations permit the ultimate tensile strength to be determined as a function of solidification processing variables. Such expressions can be used to gain insight into the foundry process, by preprogramming solidification in terms of some particular level of final mechanical properties. By using Eqs. [44] through [46], it is possible to perform simulations of the microstructure and tensile strength of an Al-4.5 wt pct Cu ingot solidifying unidirectionally under unsteady-state heat flow conditions. Figure 19 illustrates the results of the simulation for a 100-mm-long casting of an Al-4.5 wt pct Cu alloy solidified against a cooled mold with a heat transfer coefficient, $h_i = 5000$ W/m^2 K.

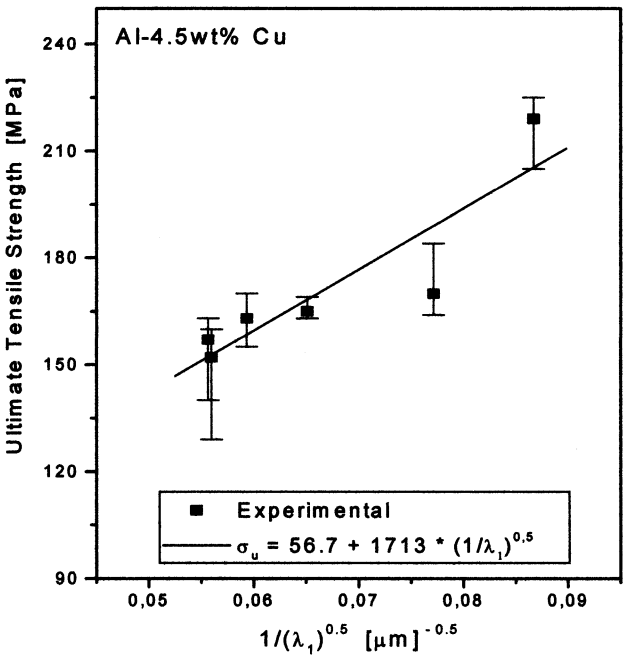

Fig. 15—Ultimate tensile strength as a function of dendrite primary spacing for Al-4.5 wt pct Cu.

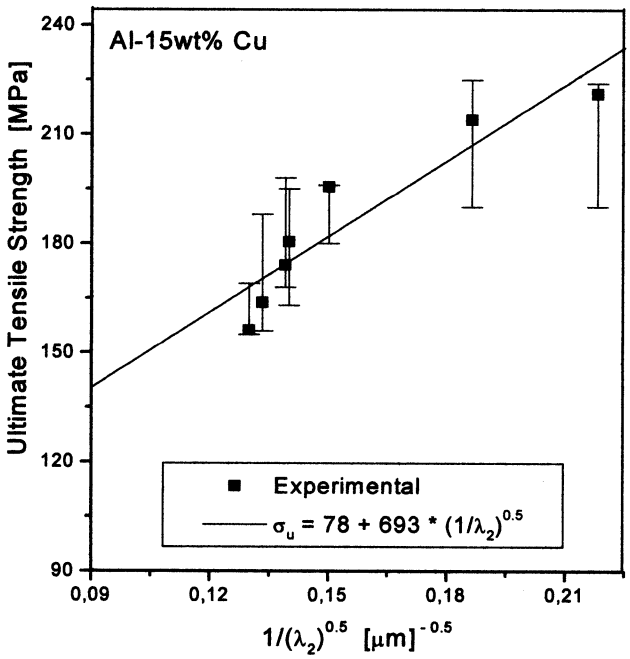

Fig. 17—Ultimate tensile strength as a function of dendrite secondary spacings for Al-15 wt pct Cu.

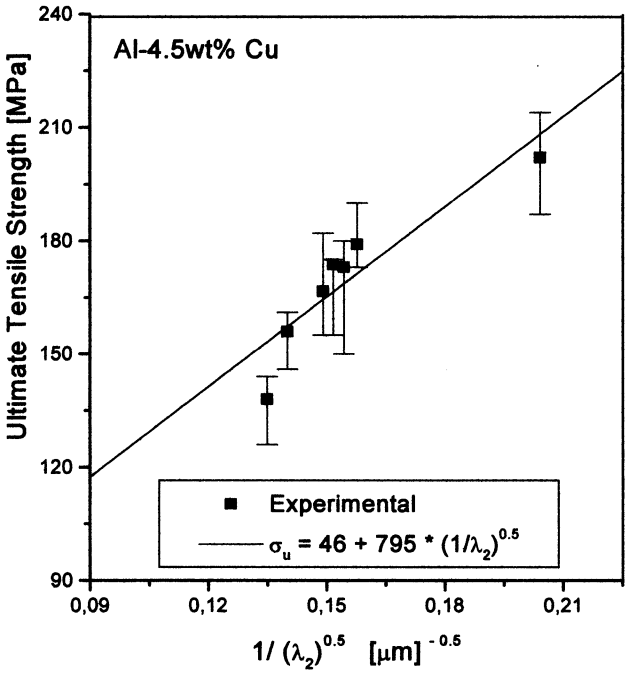

Fig. 16—Ultimate tensile strength as a function of dendrite secondary spacings for Al-4.5 wt pct Cu.

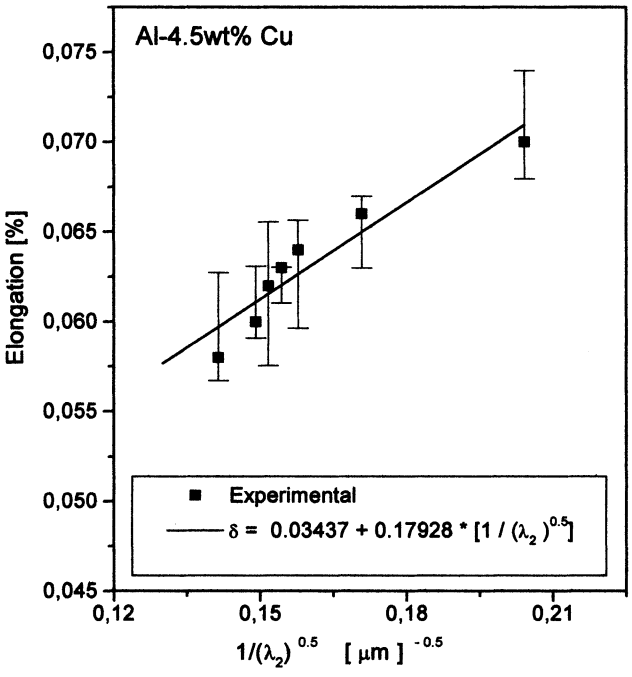

Fig. 18—Elongation as a function of dendrite secondary spacing for Al-4.5 wt pct Cu alloy.

V. SUMMARY

Analytical expressions have been developed describing thermal control parameters, *i.e.*, thermal gradients (G) and tip growth rate (V), during unsteady-state solidification of one-dimensional ingots. It was shown that the relationship between G and V is actually linear, permitting the cooling rate to be expressed only as a function of the tip growth rate. Based on the agreement between experimental and theoretically calculated dendrite spacings, the analytical expressions for the thermal control parameters were incorporated into the dendritic growth model, in order to derive general expressions, which correlate microstructure dendrite spacings with solidification processing variables. Experimental equations relating the dependence of ultimate tensile strength and ductility on dendrite spacings have been determined for Al-4.5 wt pct Cu and Al-15 wt pct Cu alloys. These equations can be expressed as a function of metal/

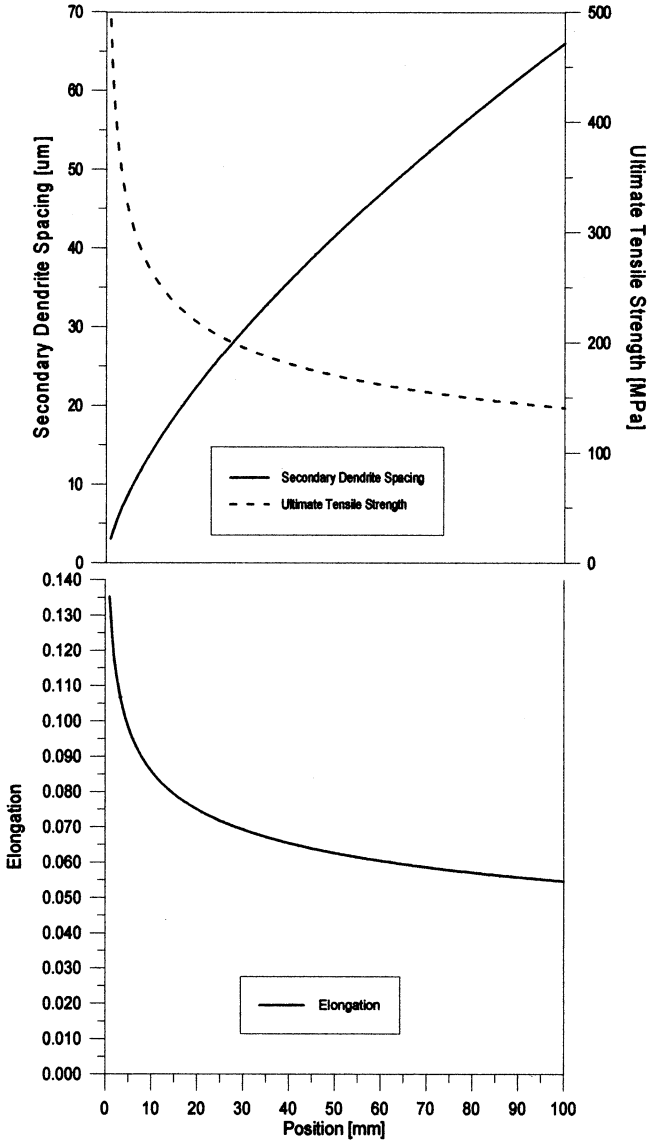

Fig. 19—Microstructure and mechanical properties simulation in a 100-mm-long unidirectional Al-4.5 wt pct Cu ingot: cooled mold and $h_i = 5000$ W/m^2 K.

mold solidification parameters and can be used on simulations of microstructure and mechanical properties.

ACKNOWLEDGMENTS

The authors acknowledge the financial support provided by FAEP-UNICAMP, FAPESP (The Scientific Research Foundation of the State of São Paulo, Brazil), and CNPq (The Brazilian Research Council).

REFERENCES

1. M. Durman: *Z. Metallkd*, 1998, vol. 6, pp. 417-23.
2. K.H.W. Seah, J. Hemanth, and S.C. Sharma: *J. Mater. Sci.*, 1998, vol. 33, pp. 23-28.
3. M.A. Savans and S. Altintas: *J. Mater. Sci.*, 1993, vol. 28, pp. 1775-82.
4. E.O. Hall: *Proc. Phys. Soc.*, 1951, vol. 71B, pp. 747-52.
5. N.J. Petch: *J. Iron Steel Inst.*, 1953, vol. 174, pp. 25-31.
6. D. Bouchard and J.S. Kirkaldy: *Metall. Mater. Trans. B*, 1996, vol. 27B, pp. 101-13.
7. J.S. Kirkaldy and D. Venugopalan: *Scripta Metall.*, 1989, vol. 23, pp. 1603-08.
8. W. Kurz and D.J. Fisher: *Acta Metall.*, 1981, vol. 29, pp. 11-20.
9. D. Bouchard and J.S. Kirkaldy: *Metall. Mater. Trans. B*, 1997, vol. 28B, pp. 651-63.
10. J.D. Hunt and S.Z. Lu: *Metall. Mater. Trans. A*, 1996, vol. 27A, p. 611-23.
11. J. Feng, W.D. Huang, X. Lin, Q.Y. Pan, T. Li, and Y.H. Zhou: *J. Cryst. Growth*, 1999, vol. 197, pp. 393-95.
12. W.W. Mullins and R.F. Sekerka: *J. Appl. Phys.*, 1964, vol. 35, pp. 444-51.
13. A. Garcia and M. Prates: *Metall. Trans. B*, 1978, vol. 9B, pp. 449-57.
14. A. Garcia, T.W. Clyne, and M. Prates: *Metall. Trans. B*, 1979, vol. 10B, pp. 85-92.
15. L.F. Mondolfo: *Aluminum Alloy—Structure and Properties*, 1st ed., Butterworth and Co, London, 1976.
16. R.D. Pehlke, A. Jeyarajan, and H. Wada: Summary of Thermal Properties for Casting Alloys and Mold Materials, The University of Michigan, Ann Arbor, MI, 1982.
17. J.T. Berry: *AFS Trans.*, 1970, vol. 78, pp. 421-28.
18. M.A. Taha, N.A. El-Mahallawy, A.W.M. Assar, and R.M. Hammouda: *J. Mater. Sci.*, 1992, vol. 27, pp. 3467-73.
19. C.A. Santos, J.M.V. Quaresma, and A. Garcia: State University of Campinas, Campinas, Brazil, unpublished research, 2000.
20. J.A. Spim and A. Garcia: *Mater. Sci. Eng. A*, 2000, vol. 277, pp. 198-05.
21. *ASTM E 8M—Standard Test Methods for Tension Testing of Metallic Materials*, ASTM, Philadelphia, PA, 1995.